Thermal Science and Engineering Progress 40 (2023) 101791

Contents lists available at ScienceDirect

Thermal Science and Engineering Progress

journal homepage: www.sciencedirect.com/journal/thermal-science-and-engineering-progress

Flow of viscoelastic ternary nanofluid over a shrinking porous medium with heat Source/Sink and radiation

T. Maranna [a], U.S. Mahabaleshwar [a], L.M. Pérez [b], O. Manca [c,*]

[a] Department of Studies in Mathematics, Davangere University, Shivagangothri, Davangere 577 007, India
[b] Departamento de Física, FACI, Universidad de Tarapacá, Casilla 7D, Arica, Chile
[c] Dipartimento di Ingegneria, Università degli Studi della Campania Luigi Vanvitelli, Aversa, CE, Italy

ARTICLE INFO

Keywords:
Viscoelastic parameter
Radiation
Inverse Darcy number
Ternary nanofluid
Solid volume fraction
Heat source/sink

ABSTRACT

Due to its extensive applicability and employment in different systems, the study of thermal transport is a significant area of research. The main goal of this investigation is to analyse the impact of thermal radiation as well as the Navier-Stokes condition upon the two-dimensional flow of second-grade as well as Walter's B ternary nanoliquids through a permeable shrinking flat surface. The phrase "ternary nanofluid" refers to a suspension of three different types of nanoparticles, notably silver (Ag), SWCNTs, and graphene particles, in water as the base fluid. The inverse Darcy phenomenon has an effect on the momentum equation as well. The energy equation also accounted for nonlinear thermal radiations as well as heat source and sink components. The phenomenon is portrayed as a nonlinear system of partial differential equations. The model equations are transformed into a non-dimensional series of ordinary differential equations by replacing similarity. Afterwards, the transformed ODEs were tackled analytically in order to establish an analytical solution of the energy equation in terms of a confluent hyper-geometric function by utilizing similarity conversion. This research reveals that the velocity field is reduced significantly by the slip parameter. The benefits of a few emerging factors, such as the viscoelastic parameter, inverse Darcy number, slip parameter, solid volume fraction, radiation, Prandtl number, and skin friction coefficient effects on solution, have been displayed through plots and discussed. Additionally, it has been concluded from this analysis that ternary nanofluids have a higher thermal flow rate than hybrid or standard nanofluids.

Introduction

Many industries use an investigation of the base and HNF streams through a permeable shrinking surface, including polymer technology, polymer extrusion, plastic sheets, compression, glass manufacturing, fiber, and metallic furnaces. Metallic nanoparticles are the most beneficial due to their better thermal conductivity than other types of liquids. The effect of nanofluid size, structure, concentration, and thermophysical properties on heat transmission rate was thoroughly investigated. Due to their fascinating thermal properties and possible uses, this study area has inspired a lot of attention among scientists. Ekiciler [1], a steady fluid referred to as nanoparticles, is built by a specific group of nanoparticles in a base liquid. However, a hybrid nanofluid develops when there are two different types of nanomaterials. Lately, additional research into nanofluid has involved the circulation of three different kinds of nanoparticles in a base liquid to generate steady tnf. Later, researchers conducted extensive research on nanofluids [2–3]. Efficiency for heat transfer utilizing nanofluids is frequently better than with commonly used liquids such as oil and ethylene glycol. HNFs have drawn considerable attention due to their enhanced heat transmission capabilities. Obviously, the most well-known concern with heat exchangers is the problem of heat transfer. Using a variety of water-based tnf ($Al_2O_3 + Cu + CNT$) nanoparticles, Sahu [4] investigated the free convective stable and loop transient properties.

In order to accelerate the process of heat transport, Xuan [5] incorporated thermal dispersion into the motion. The researchers proposed two approaches for evaluating the nanofluid thermal transfer relationship. Afterwards, Xuan [6] provided a conceptual pattern to demonstrate the characteristics of nanoparticle heat transfer circulating through tubular sectors. An objective of synthesizing nanofluid composites is to enhance the rheological or thermal performance of individual nanoparticles by integrating them into a homogeneous nanoparticle with improved properties. The heat capacity as well as the

* Corresponding author.
E-mail addresses: u.s.m@davangereuniversity.ac.in (U.S. Mahabaleshwar), lperez@academicos.uta.cl (L.M. Pérez), oronzio.manca@unicampania.it (O. Manca).

https://doi.org/10.1016/j.tsep.2023.101791
Received 16 December 2022; Received in revised form 19 January 2023; Accepted 8 March 2023
Available online 11 March 2023

Nomenclature

A	slip length (m)
c	Constant (-)
C_p	Specific heat ($JK^{-1}kg^{-1}$)
Da^{-1}	Inverse Darcy number (-)
$1F1$	Confluent hypergeometric function (-)
f	Similarity function (-)
K	Viscoelastic factor (-)
K_1	Permeability (N/A^2)
k^*	Coefficient of viscoelastic (-)
k_1	Mean absorption factor (-)
N_r	Radiation parameter (-)
N_I	Heat source/sink factor (-)
Pr	Prandtl number (-)
Q_0	Heat generation/absorption coefficient (-)
q_r	Radiative heat flux (Wm^{-2})
T	Temperature of the fluid (K)
T_w	Wall temperature (K)
T_∞	Ambient temperature (K)
u, v	Components of velocities along $\times$ and y-axes (m/s)
x, y	Horizontal and vertical axes(-)

Greek symbols

α	Constant (-)
λ	First order slip (-)
κ_f	Thermal conductivity ($Wm^{-1}K^{-1}$)
μ_f	Absolute viscosity ($Ns\ m^{-2}$)
η	Similarity variable (-)
ψ	Stream function (-)
ρ_f	Density of base fluid ($kg\ m^{-3}$)
σ^*	Stefan-Boltzmann constant ($Wm^{-2}K^{-4}$)
ϕ	Solid volume fraction of the nanoparticles (-)

Subscripts

f	Base fluid (-)
tnf	Ternary nanofluid (-)

Abbreviations

ODEs	Ordinary differential equations
PDEs	Partial differential equations
HNF	Hybrid nanofluid

rheological characteristics of final nanocomposites can be developed via the construction of a mixture of nanoparticles. It is assured through the creation of the perfect mixture of nanostructures. It's possible that a nanofluid prepared by incorporating nanoparticles with great thermal conductivity may not also have stronger rheological characteristics. As a result, introducing nanomaterials with various rheological or thermal properties strengthens the nanofluids overall effectiveness and makes it more steady as well as efficient.

The most effective performance is exhibited by nanoparticles in their specific patterns. Several studies [7–8] have looked attentively at the physics and applications of hybrid TiO_2, MgO, and $CoFe_2O_4$ NF over a spectrum of configurations. Currently, Maranna [9] scrutinizes the role of heat radiation, mass suction or blowing, as well as Marangoni barrier constraints, on the stream of ternary nanoparticles in a permeable material. Besides straightening surfaces with penetrable materials, there is an unstable motion of coupled stress through a tnfs, as researched by Sneha [10]. Furthermore, because of their significant qualities that increase heat transfer rates, nanoparticles are frequently used in production and for industrial purposes.

Gul [11] investigated how to improve the thermal circulation of trihybrid nanoparticles flowing along a nonlinear extendable surface. It was demonstrated that when volumetric proportions of nanoparticles increase, the velocity profile and non-linearity indices of the surface decrease. Hypothetically, Manjunatha [12] addresses heat transmission in ternary nanoparticles (TiO_2-SiO_2-Al_2O_3/H_2O) streaming across a stretching sheet. Numerous studies [13–15] have shown that nanofluid significantly improves heat transmission when compared to conventional heat transfer materials. A boundary layer flow analysis is extremely helpful from a physical perspective because it has so many applications. It ought to be emphasized that free stream flow through fixed plates differs greatly from boundary layer flow across surfaces [16,17].

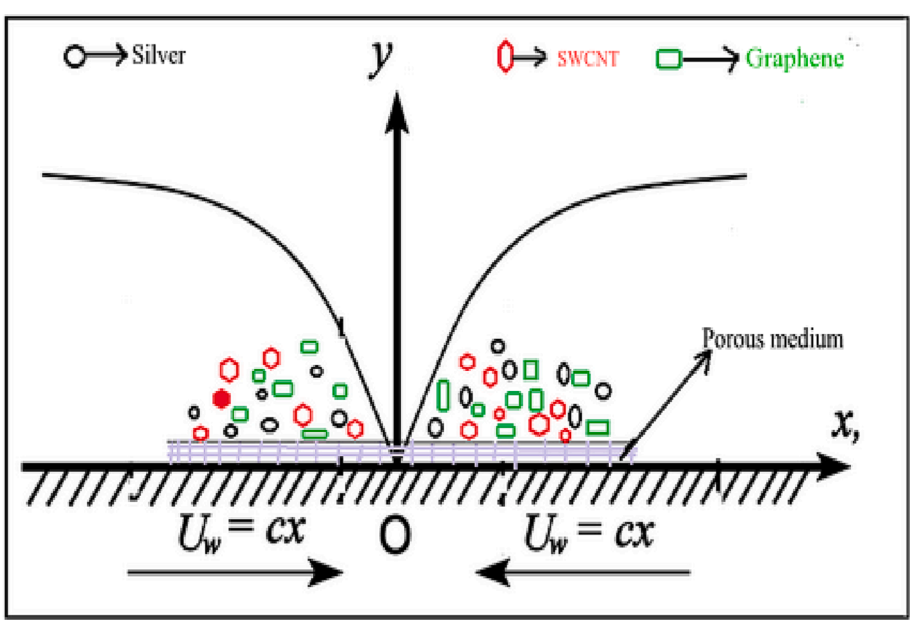

Fig. 1. Fig. 1: Schematic representation of the flow problem.

Table 1
Table1-1: Properties of base fluid and nano particles numerical values [52–55].

Properties	H_2O	Silver (Ag)	SWCNTs	Graphene
$\rho(kgm^{-3})$	997.1	10,500	2600	2200
$\kappa\left(wm^{-1}k^{-1}\right)$	0.613	429	6000	5000
$C_p(JKg^{-1}K^{-1})$	4180	235	425	790

Numerous researchers [18–20] used the boundary layer model to investigate mass and temperature transport under a variety of conditions, such as the operating fluid's non-Newtonian behavior, heat flux, surrounding heaters, suction/injection, velocity slip, and porous materials. Due to its growing use in solving numerous technical challenges, the stream of viscous, incompressible liquid owing to a contraction plate has gained importance in recent years among modern researchers. Beyond diminishing surface, Hayat [21] explained the analytical MHD stream of 2nd grade liquid. The motion of a viscoelastic liquid past an elongated surface has been examined by Rajagopal [22].

In light of many physical problems, it is crucial to investigate how heat sources and sinks affect heat transport. Restricted to the situation of viscous liquids alone, Emad [23] has considered the influence of an unsteady heat source along with suction or injection. An impact of radiation upon motions including a viscoelastic fluid has been studied by several researchers [24–25], who discuss the impact of radiation in different contexts. Moreover, all studies were conducted with consistent physical parameters and a continuous heat source. Empirical research [26] has been done on the thermal efficiency of several hybrid nanoparticles on the heat sink for a small hexagonal pipe. The interaction between chemical radiation, heat generation and absorption by viscous fluid movement, and mass transpiration at a thermosolutal Marangoni perforated interface is studied by Mahabaleshwar [27]. Very recently, Debasish [28] investigates the characteristics of dual solutions in magnetohydrodynamic boundary layer flow of a conducting fluid through an exponentially stretching/shrinking sheet with simultaneous temperature and concentration distribution in a porous material. Babu [29] addresses the heat transfer properties of an incompressible non-Newtonian Jeffrey fluid over a shrinking/stretching surface using thermal radiation and a heat source. The features of a magnetite ferrofluid flowing past a stretchable/decreasing sheet in a Darcy-Forchheimer porous material with viscous and porous dissipation as well as convective heating effects and the combined effects of a magnetic field, thermal radiation, convective heating, and buoyant force on the flow of an electrically conducting nanofluid through a stretchable/contractible sheet in a porous material at its stagnation point are studied by Tadesse [30–31]. Furthermore, Jamuna [32] presented a solution of dualities in electrically conductive nanofluids correlated to melting phenomena across a stretching/shrinking sheet. In the meanwhile, one of the least expensive ways to determine whether a nonlinear problem's solution branch is physically feasible is to conduct stability analysis for several solutions. Investigation of stability and dual solutions for the flow of heated shrinking/stretching surfaces using magneto-nanofluids by Tshivhi [33]. Using the Dirichlet series and the method of stretching factors, the nonlinear problem of Casson fluid flow through a permeable stretching/shrinking sheet is addressed by Makinde [34].

Inspired by all of these aforementioned literatures, we interested to study an impact of thermal radiation, Navier slip with unsteady heat source/sink on 2D motion of viscoelastic ternary nanoparticles flow past a permeable shrinking plate. This article addresses 2nd as well as viscous elastic liquid behavior. Here fluid flow is stretched using a porous material. Because the use of fluid movement in porous media is widespread in industry. Mass suction is typically used to ensure consistent flow on a permeable surface that is constricting. While in the current analysis, partial slip is taken into account simultaneously to investigate the situations under which a steady-state solution exists and does not.

Additionally, the impact of partial slip on the uniqueness as well as the non-uniqueness of responses is investigated. Through similarity conversions, the dominating equations for the boundary layer are modified into a series of ODEs. The derived expressions were solved analytically. Velocity, temperature, and skin friction have been evaluated for variation in the different governing parameters. The below factors will strengthen the originality among the issue:

(i) Three different sorts of nanofluids—Ag, SWCNTs, and Graphene are spread throughout the base fluid, which is water.
(ii) The flow model incorporates nonlinear thermal radiations as well as heat absorption/ generation factors.
(iii) The flow system takes the Darcy phenomenon into account.
(iv) Our prime objective seems to be to investigate features of ternary nanofluid motion for commercial and biological implications. Long-term, this study may have been employed to evolve a required heating method that utilizes suitable physical sources, such as refrigerants and heat pumps.

Mathematical modelling

Consider the steady two - dimensional flow of Walters' B fluid as well as incompressible second-grade liquid across a shrinking porous sheet with first order slip. In order to confine the flow zone $y > 0$, the shrinking flat sheet is drawn along the plane $y = 0$. Through the application of two equal and inverted forces along the x-axis, while preserving the origin's location, movement is formed for the shrinking of a flat surfaces. where the flat surface contraction velocity is $U_w(x) = \alpha x$. A sketch of the problem is depicted in Fig. 1.

The fundamental equations which govern the flow of ternary nanofluids are described [35–38] as follows:

Continuity equation:

$$\frac{\partial u}{\partial x}+\frac{\partial v}{\partial y} = 0, \tag{1}$$

Momentum equation:

$$u\frac{\partial u}{\partial x}+v\frac{\partial u}{\partial y} = \frac{\mu_{tnf}}{\rho_{tnf}}\frac{\partial^2 u}{\partial y^2}\pm k^*\left\{u\frac{\partial^3 u}{\partial x\partial y^2}+\frac{\partial u}{\partial x}\frac{\partial^2 u}{\partial y^2}+v\frac{\partial^3 u}{\partial y^3}-\frac{\partial u}{\partial y}\frac{\partial^2 u}{\partial x\partial y}\right\}-\frac{\mu_{tnf}}{\rho_{tnf}K_1}u, \tag{2}$$

Energy equation:

$$u\frac{\partial T}{\partial x}+v\frac{\partial T}{\partial y} = \frac{\kappa_{tnf}}{(\rho C_p)_{tnf}}\frac{\partial^2 T}{\partial y^2}+\frac{Q_0(T-T_\infty)}{(\rho C_p)_{tnf}}-\frac{1}{(\rho C_p)_{tnf}}\frac{\partial q_r}{\partial y}, \tag{3}$$

with imposed boundary constraints [39–41] are

$$\begin{aligned} &u = -U_w(x)+A\frac{\partial u}{\partial y},\quad v = 0,\quad T = T_w \qquad \text{at } y = 0,\\ &u\to 0,\quad \frac{\partial u}{\partial y}\to 0,\quad T = T_\infty, \qquad \text{as } y\to\infty. \end{aligned} \tag{4}$$

here A be the slip length.

Dimensionless ruling conversations

Through resemblance transformations, the governing PDEs are transformed into ODEs. [39,42,43].

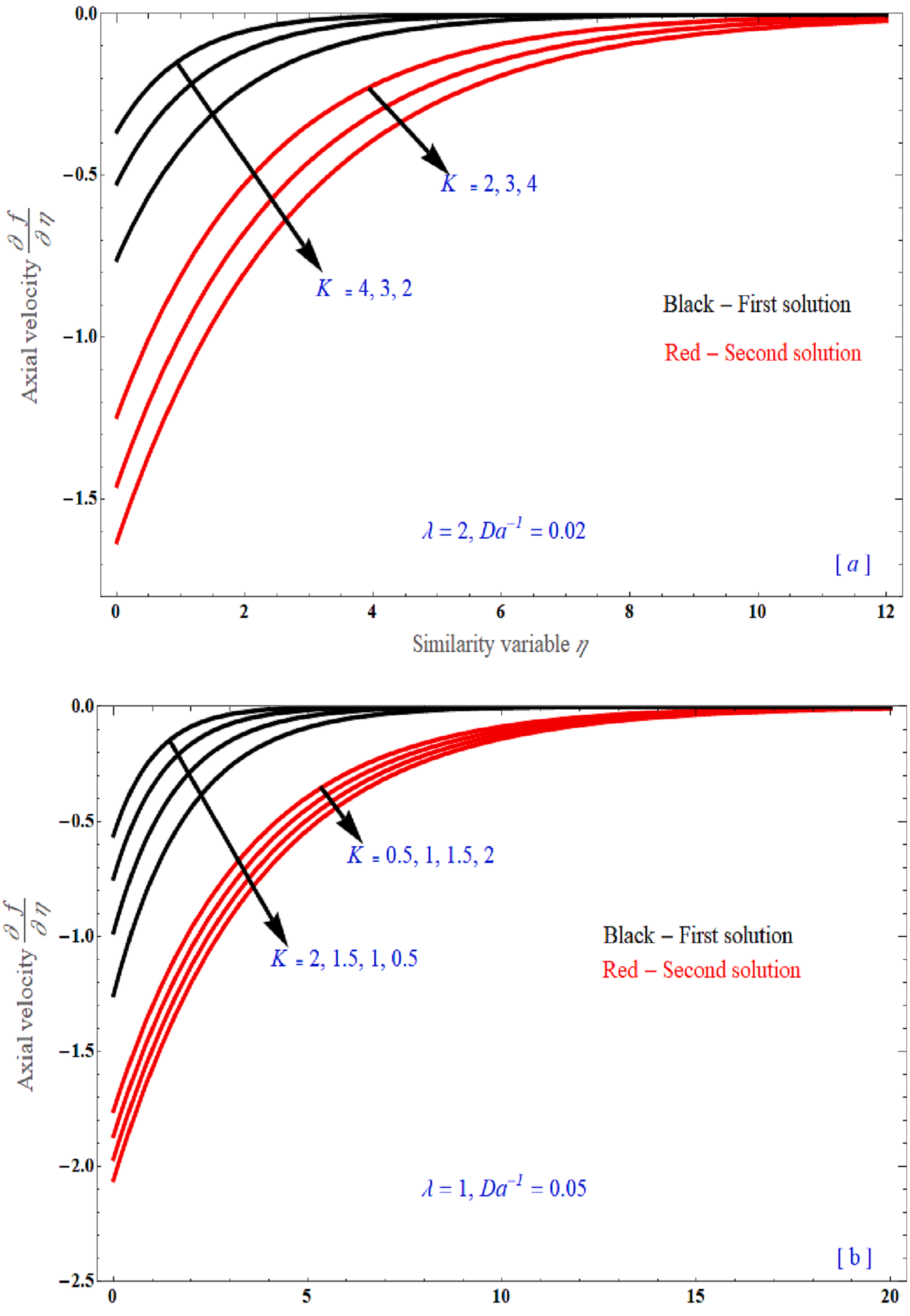

Fig. 2. An impact of viscoelastic parameter K on axial velocity with (a) $\lambda = 2$ and (b)$\lambda = 1$..

$$\psi = \sqrt{\nu_f x U_w x} f(\eta), \quad \eta = \sqrt{\frac{U_w(x)}{\nu_f x}} y,$$
$$u = \frac{\partial \psi}{\partial y} = \alpha x f'(\eta), \quad v = \sqrt{\nu_f \alpha} f(\eta), \tag{5}$$
$$T = T_\infty + (T_w - T_\infty)\theta(\eta).$$

aforementioned (u, v) interpret components of flow across (x, y) -axes respectively. Furthermore, μ_{tnf}, ρ_{tnf}, κ_{tnf} and $(\rho C_p)_{tnf}$ are entitle as dynamic viscosity, density, thermal conductivity as well as heat capacitances of ternary nanofluid. While α is the constant with ν_f be the base liquid kinematic viscosity, k^* to be viscoelastic factor and K_1 is the permeability of the porous medium. Description of the other parameters is mentioned in the nomenclature section.

The radiative heat flux q_r is narrated [44–47] as

$$q_r = -\frac{4\sigma^*}{3k_1}\frac{\partial T^4}{\partial y}, \tag{6}$$

where σ^* and k_1 stands for Stefan-Boltzmann constant and Rosseland mean absorption coefficient, correspondingly. Apparently, the temperature variations inside flow are negligible slightly, in such a way that T^4

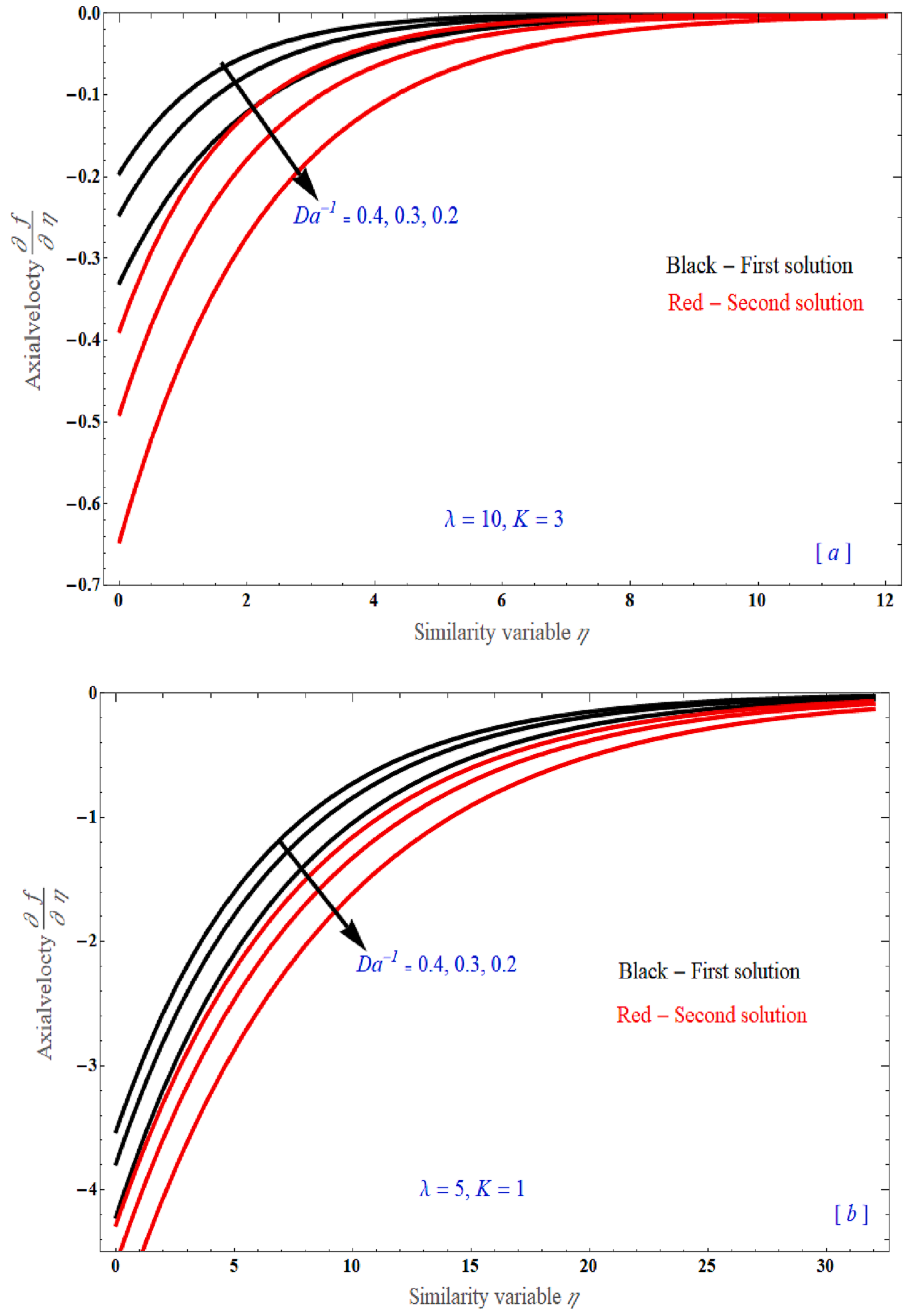

Fig. 3. An impact of inverse Darcy factor Da^{-1} on axial velocity with (a) $\lambda = 10$ and (b) $\lambda = 5$.

can stated as a linear function of temperature and neglecting the higher order term.

$$T^4 \approx 4T_\infty^3 - 3T_\infty^4, \tag{7}$$

employing Eqn. (6) and (7) in Eqn. (3), we obtain

$$\frac{\partial q_r}{\partial y} = -\frac{16\sigma^* T_\infty^3}{3k_1}\frac{\partial^2 T}{\partial y^2}, \tag{8}$$

currently, Eqn. (3) be rewritten as

$$u\frac{\partial T}{\partial x} + v\frac{\partial T}{\partial y} = \frac{\kappa_{tnf}}{(\rho C_p)_{tnf}}\frac{\partial^2 T}{\partial y^2} + \frac{Q_0}{(\rho C_p)_{tnf}} + \frac{1}{(\rho C_p)_{tnf}}\frac{16\sigma^* T_\infty^3}{3k_1}\frac{\partial^2 T}{\partial y^2}, \tag{9}$$

For spherical, cylindrical, as well as platelet nanoparticle, the dynamic viscosity, thermal conductivity, density, and heat capacity characteristics are [48–51] stated by

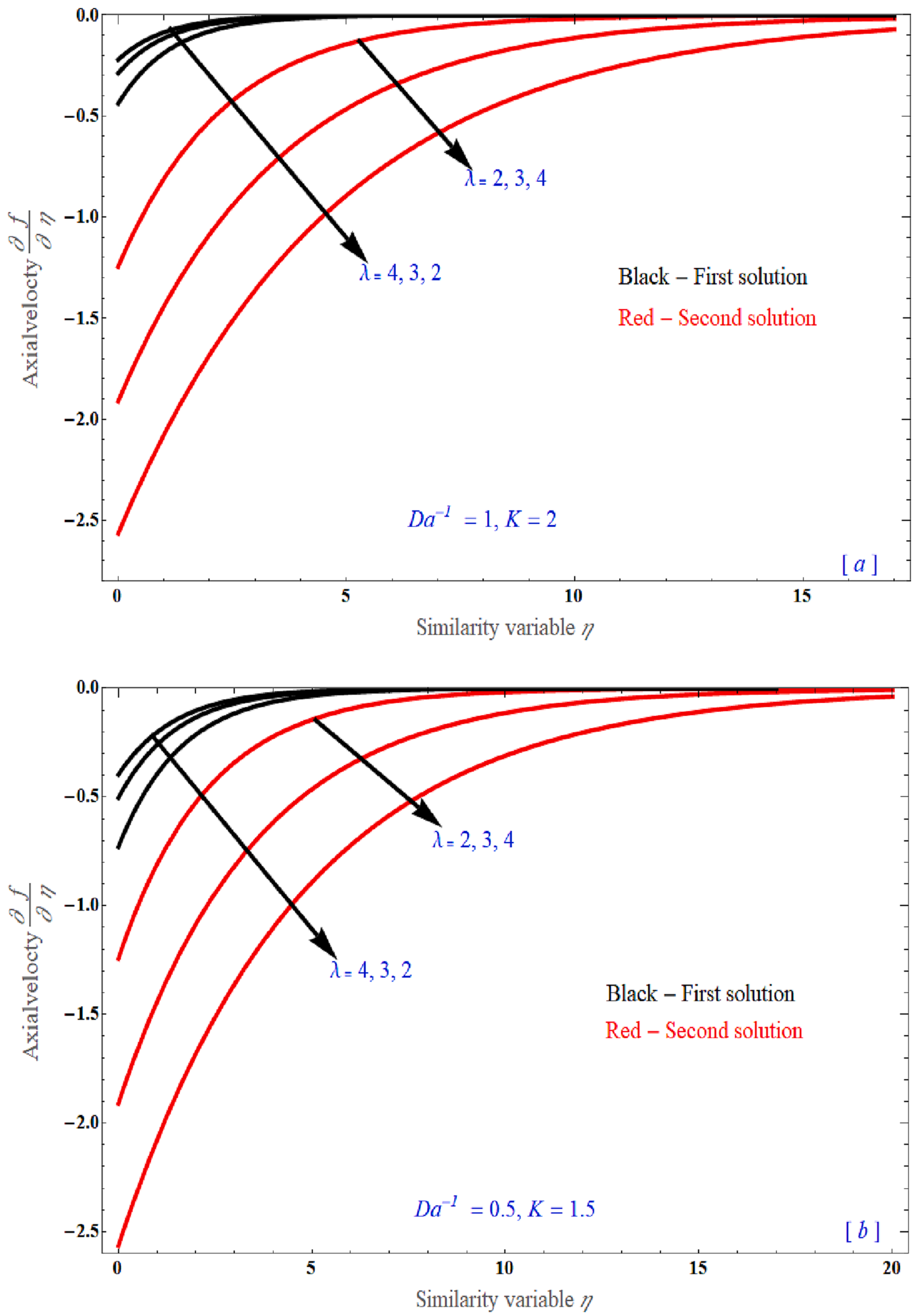

Fig. 4. An impact of slip parameter λ on Axial velocity parameter with (a)$Da^{-1} = 1$ and (b) $Da^{-1} = 0.5$.

$$\mu_{tnf} = \frac{\mu_{nf1}\phi_1 + \mu_{nf2}\phi_2 + \mu_{nf3}\phi_3}{\phi},$$

$$\rho_{tnf} = \rho_{sp1}\phi_1 + \rho_{sp2}\phi_2 + \rho_{sp3}\phi_3 + (1-\phi_1-\phi_2-\phi_3)\rho_f,$$

$$\kappa_{tnf} = \frac{\kappa_{nf1}\phi_1 + \kappa_{nf2}\phi_2 + \kappa_{nf3}\phi_3}{\phi},$$

and

$$(\rho C_p)_{tnf} = (\rho C_p)_{sp1}\phi_1 + (\rho C_p)_{sp2}\phi_2 + (\rho C_p)_{sp3}\phi_3 + (1-\phi_1-\phi_2-\phi_3)(\rho C_p)_f. \tag{10}$$

For spherical nanoparticles, the effective viscosity as well as thermal conductivity is given by

$$\frac{\mu_{nf_1}}{\mu_f} = 1 + 2.5\phi + 6.2\phi^2, \frac{k_{nf_1}}{k_f} = \left(\frac{k_{sp_1} + 2k_f - 2\phi(k_f - k_{sp_1})}{k_{sp_1} + 2k_f + \phi(k_f - k_{sp_1})}\right), \tag{11}$$

Cylindrical nanoparticle quantities,

$$\frac{\mu_{nf_2}}{\mu_f} = 1 + 13.5\phi + 904.4\phi^2, \frac{k_{nf_2}}{k_f} = \left(\frac{k_{sp_2} + 3.9k_f - 3.9\phi(k_f - k_{sp_2})}{k_{2sp_2} + 3.9k_f + \phi(k_f - k_{sp_2})}\right), \tag{12}$$

Platelet nanoparticles quantities,

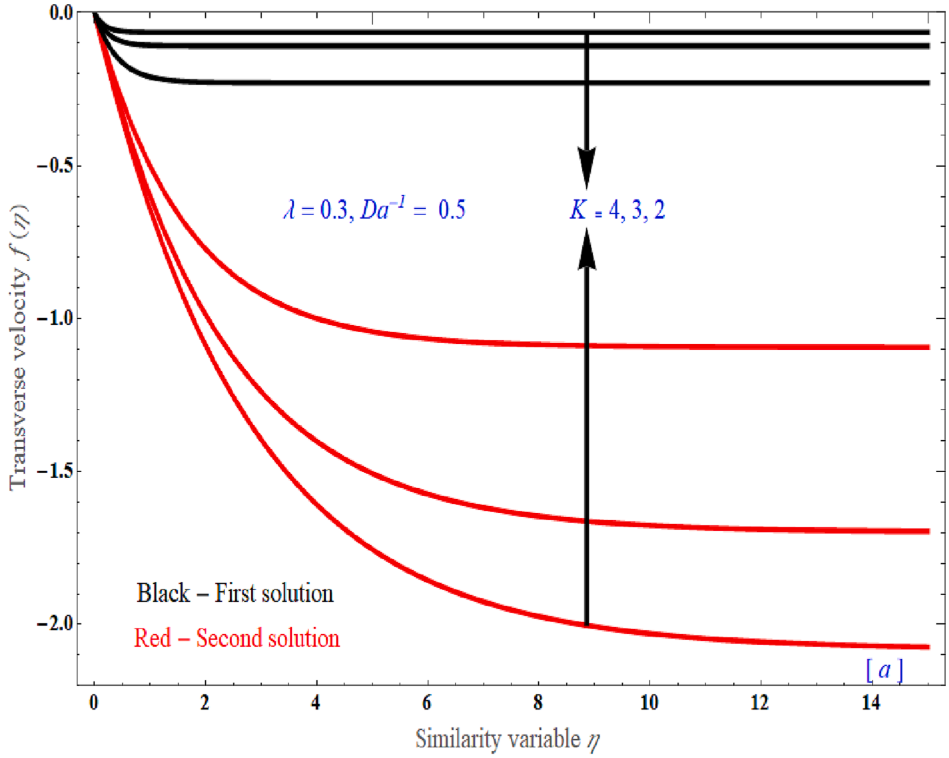

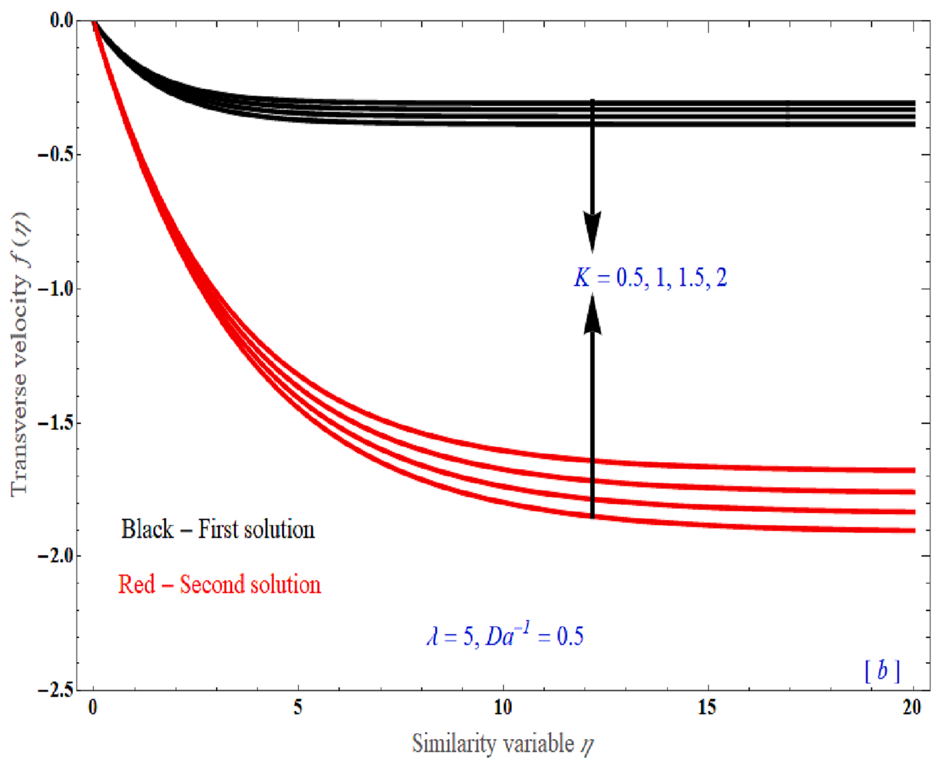

Fig. 5. An impact of viscoelastic parameter K on axial velocity with (a) $\lambda = 0.3$ and (b)$\lambda = 5$.

$$\frac{\mu_{nf_3}}{\mu_f} = 1 + 37.1\phi + 612.6\phi^2, \frac{k_{nf_3}}{k_f} = \left(\frac{k_{sp_3} + 4.7k_f - 4.7\phi(k_f - k_{sp_3})}{k_{2sp_3} + 4.7k_f + \phi(k_f - k_{sp_3})}\right), \tag{13}$$

here $\phi = \phi_1 + \phi_2 + \phi_3$, in which ϕ_1, ϕ_2 and ϕ_3 are the solid volume fraction of the spherical, cylindrical and platelet nanoparticles respectively. The property values of the base fluid and three nanoparticles are given in Table 1.

Eqn. (5) can be incorporated into Eqn. (2) and (9) to produce the resulting system of nonlinear ODEs as

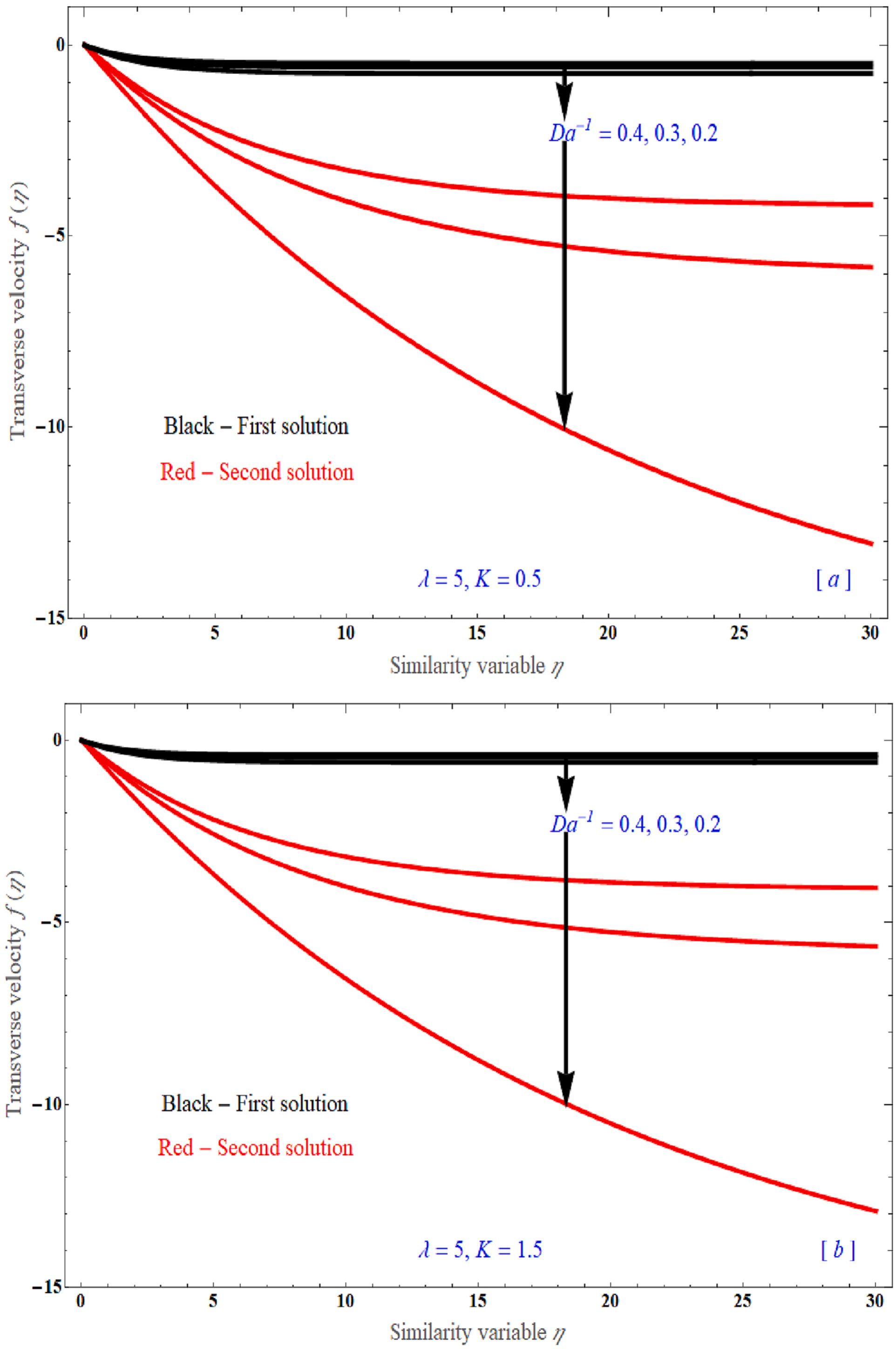

Fig. 6. An impact of inverse Darcy factor Da^{-1} on transverse velocity with (a) $K = 0.5$ and (b) $K = 1.5$.

$$\frac{\xi_1}{\phi}f''(\eta) - K\xi_2\{f(\eta)f^{iv}(\eta) - (f''(\eta))^2 - 2f'(\eta)f''(\eta)\} + \{f(\eta)f''(\eta) - (f'(\eta))^2\} - \frac{\xi_1}{\phi}Da^{-1}f'(\eta) = 0, \tag{14}$$

$$(\xi_3 + N_r)\theta'' + \xi_4 Prf\theta'(\eta) + PrN_I\theta(\eta) = 0, \tag{15}$$

In above system of equations,

$\xi_1 = \frac{\mu_{tnf}}{\mu_f}$, $\xi_2 = \frac{\rho_{tnf}}{\rho_f}$, $\xi_3 = \frac{\kappa_{tnf}}{\kappa_f}$, with $\xi_4 = \frac{(\rho C_p)_{tnf}}{(\rho C_p)_f}$ are the thermo-physical symbols, viscoelastic parameter is denoted as $K = \frac{\alpha k^*}{\nu_f}$ with $K > 0$ stands for second grade fluid and $K < 0$ for Walters' liquid B, respectively. Inverse Darcy number can be termed as $Da^{-1} = \frac{\nu_f}{\alpha K_1}$, $Pr = \frac{\mu_f C_p}{\kappa_f}$ is the Prandtl number with $N_I = \frac{Q_0 a^2}{\nu_f (\rho C_p)_f}$ be the heat source/sink parameter correspondingly.

Modified boundary conditions are given below:

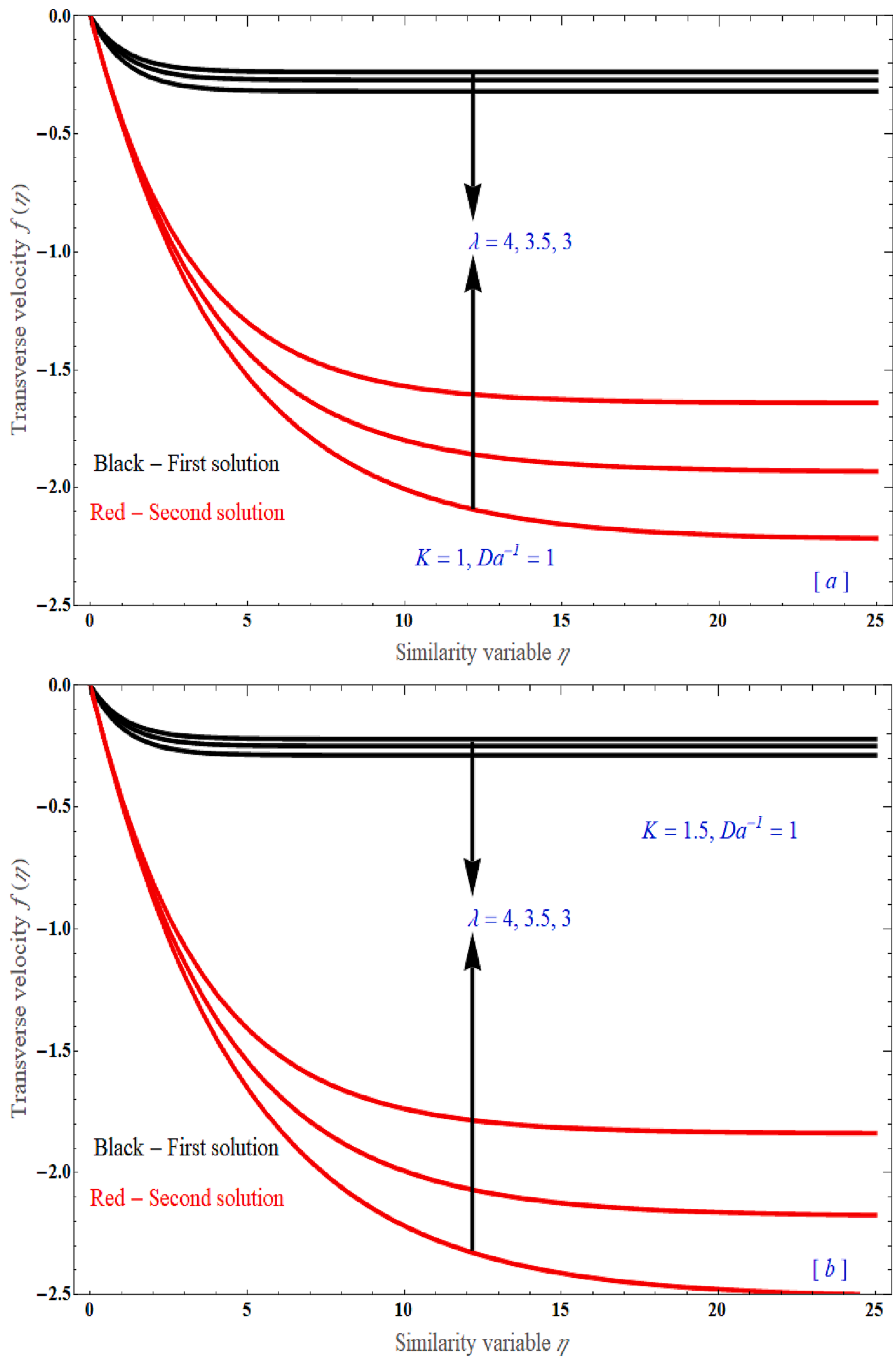

Fig. 7. An impact of Navier slip parameter λ on transverse velocity with (a) $K = 1$ and (b) $K = 1.5$.

$$\left(\frac{\partial f}{\partial \eta}\right)_{\eta\to 0} = -1+\lambda\left(\frac{\partial^2 f}{\partial \eta^2}\right)_{\eta\to 0},\ f(\eta)_{\eta\to 0} = 0,\ \ \theta(\eta)_{\eta\to 0} = 1,$$
$$\left(\frac{\partial f}{\partial \eta}\right)_{\eta\to\infty} = 0,\ \left(\frac{\partial^2 f}{\partial \eta^2}\right)_{\eta\to\infty} = 0,\ \ \theta(\eta)_{\eta\to\infty}\to 0. \tag{16}$$

here $\lambda = A\sqrt{\frac{\alpha}{\nu_f}}$ is the slip parameter.

Quantities of interest

Regarding the current model, C_f is important engineering physical parameters which is referred to as

$$C_f = \frac{\tau_w}{1/2\rho_{tnf}U_w^2}, \tag{17}$$

here

$$\tau_w = \rho_{tnf}\left\{\nu_{tnf}\frac{\partial u}{\partial y}\pm k^*\left(2\frac{\partial u}{\partial x}\frac{\partial u}{\partial y}+u\frac{\partial^2 u}{\partial x\partial y}\right)\right\}_{y=0}, \tag{18}$$

hence, skin friction C_f is determined as

$$\frac{1}{2}Re_x^{\frac{-1}{2}}C_f = \left\{\frac{\xi_1}{\xi_2}-3K\left(1-\lambda\left\{\frac{\partial^2 f}{\partial\eta^2}\right\}_{\eta=0}\right)\right\}\left\{\frac{\partial^2 f}{\partial\eta^2}\right\}_{\eta=0}, \tag{19}$$

where $Re_x = \frac{U_w x}{\nu_f}$ be designate as local Reynolds number.

Solution of momentum problem

The exact solution to the Eqn. (14), implementing the barrier constraints (16), be formed as

$$f(\eta) = \frac{-1+e^{-\beta\eta}}{\beta+\lambda\beta^2}, \tag{20}$$

Plugging Eq. (20) for dimensionless similarity in Eqn. (14) yields the following third-order algebraic polynomial, which may be interpreted as

$$\frac{\xi_1}{\phi}\lambda\beta^3+(\xi_1-3K\xi_2)\beta^2-\frac{\xi_1 Da^{-1}\lambda\beta}{\phi}+\xi_2-\frac{\xi_1 Da^{-1}}{\phi} = 0, \tag{21}$$

Eq. (21) can be modified as

$$a\beta^3+b\beta^2-e\beta+d=0, \tag{22}$$

where

$$a = \frac{\xi_1\lambda}{\phi},\ \ b = (\xi_1-3K\xi_2),\ \ c = \frac{\xi_1 Da^{-1}\lambda}{\phi}\ \text{ and }\ d = \xi_2-\frac{\xi_1 Da^{-1}}{\phi}.$$

The roots of the above Eq. (22) is presented as

$$\beta_1 = \frac{2^{\frac{1}{3}}e}{\left(-27a^2d-54abd-27b^2d+\sqrt{-108(a+b)^3e^3+\left(-27a^2d-54abd-27b^2d\right)^2}\right)^{\frac{1}{3}}}+\frac{\left(-27a^2d-54abd-27b^2d+\sqrt{-108(a+b)^3e^3+\left(-27a^2d-54abd-27b^2d\right)^2}\right)^{\frac{1}{3}}}{3*2^{\frac{1}{3}}(a+b)},$$

$$\beta_{2,3} = -\frac{(1\pm i\sqrt{3})e}{2^{\frac{1}{3}}\left(-27a^2d-54abd-27b^2d+\sqrt{-108(a+b)^3e^3}+\left(-27a^2d-54abd-27b^2d\right)^2\right)^{\frac{1}{3}}}+\frac{(1\mp i\sqrt{3})\left(-27a^2d-54abd-27b^2d+\sqrt{-108(a+b)^3e^3}+\left(-27a^2d-54abd-27b^2d\right)^2\right)^{\frac{1}{3}}}{6*2^{\frac{1}{3}}(a+b)}, \tag{23}$$

Additionally, the presented problem has two solutions, as seen by the three different roots listed above.

Exact solution for heat transfer problem

In order to solve Eqn. (15) together with boundary constraints (16), we introduced new variable as $t = \frac{Pr}{\beta^2}e^{-\beta\eta}$ which will provide

$$t\frac{\partial^2\theta}{\partial t^2}+(1+m-nt)\frac{\partial\theta}{\partial\eta}+\frac{\Gamma}{t}\theta(t) = 0, \tag{24}$$

here

$m = \frac{\xi_4 Pr}{\beta^2(1+\lambda\beta)(\xi_3+N_r)}$, $n = \frac{\xi_4}{(1+\lambda\beta)(\xi_3+N_r)}$ and $\Gamma = \frac{N_I Pr}{\beta^2(\xi_3+N_r)}$.

Next, the associated boundary conditions (16) are converted to

$$\theta\left(\frac{Pr}{\beta^2}\right) = 1,\ \ \theta(0) = 0. \tag{25}$$

By supposing that Eq. (24) has a power series solution $\theta(t) = \sum_{r=0}^{\infty}a_r t^{r+p}$ by applying the Frobenius approach, the exact solution in perspective of t can be found as

$$\theta(t) = a_0 t^{p_1+p_2}1F1\left\{\frac{p_1+p_2}{2},p_2+1,\ nt\right\}, \tag{26}$$

In aspects of η, the solution will be

$$\theta(\eta) = a_0 t^{\frac{p_1+p_2}{2}}1F1\left\{\frac{p_1+p_2}{2},p_2+1,\ nt\right\}, \tag{27}$$

By employing the boundary conditions i.e. $\theta\left(\frac{Pr}{\beta^2}\right) = 1$, we have solution in terms of Kummer's confluent hypergeometric function as follows

$$\theta(\eta) = \left(\frac{t}{t_0}\right)^{\frac{p_1+p_2}{2}}\left\{\frac{1F1\left(\frac{p_1+p_2}{2},\ p_2+1,\ nt\right)}{1F1\left(\frac{p_1+p_2}{2},\ p_2+1,\ nt_o\right)}\right\}, \tag{28}$$

which is the required solution of the proposed problem, next section we

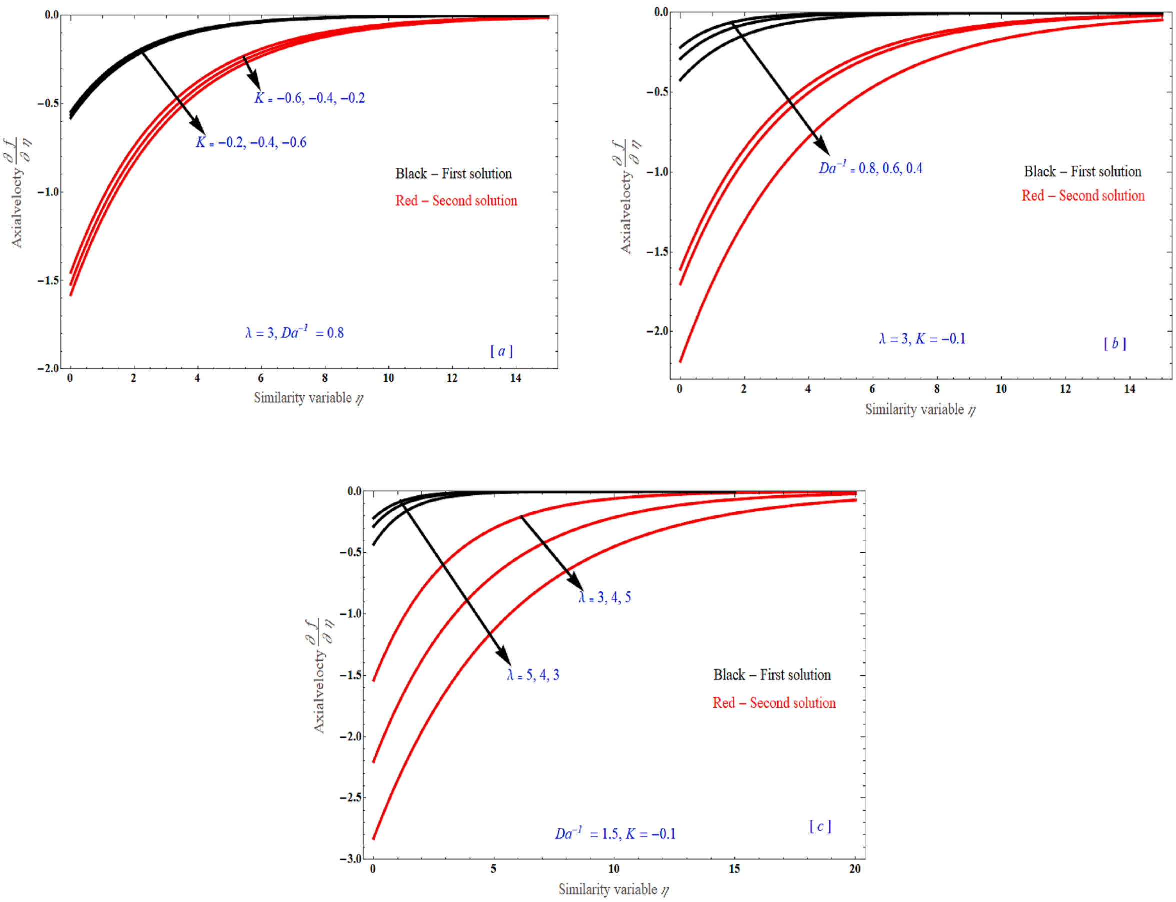

Fig. 8. An impact of (a) viscoelastic parameter K (b) inverse Darcy parameter Da^{-1} and (c) Navier slip λ on axial velocity.

will discussion about the results of the current problem.

Results and discussion

In the latest research, the flow of viscoelastic incompressible ternary nanofluid through contraction surface via a porous media is taken into consideration while thermal radiation, the Navier slip condition, and a steady heat source / sink are all included. The non - isothermal heat transmission scenario is strongly influenced by the heat generation /absorption. The porous media are another factor taken into account in this investigation. A thermal body is frequently insulated using porous medium, to keep it at a constant temperature. The looking upon inspection of momentum as well as energy equations, that produces collection of ordinary differential equations, further simplifies the exploration. By employing the proper resemblance variable, precise exact solutions for momentum as well as energy patterns can be obtained. These outcomes are validated by comparing it with those existing in the literature [32]. Different physical characteristics and pictorial configurations can be used to evaluate the outcomes of the current attempt.

The significance of viscoelastic coefficient K_1 upon velocity profile with η is reviewed in Fig. 2 (a)-(b) and Fig. 5 (a)-(b). As may be seen, the velocity profile decreases as enhances the magnitude of viscoelastic parameter in the 2nd branch solution for 2nd grade fluid. Where as in 1st branch solution reverse process is occurred. This indicates that the horizontal velocity is decreased due to the influence of the viscoelastic parameter, which also diminishes the width of barrier layer. Hence, greater strength of K contributes to a diminishes in boundary layer width. whereas reverse effect is observed for Fig. 5(b) as compared to Fig. 2(a)-(-b) and Fig. 5(a).

Fig 3(a)-(b) and Fig. 6 (a)-(b) depicts the velocity profile for various values of the inverse Darcy number for various conditions of. From this graph, It is evident that the velocity profile enhances as the inverse Darcy number goes up. Physically, this results from the fact that an elevation in values,induces a reduction in the permeability of porous material, which predicts greater resistance to flow owing to the presence of porous fibre, as well as creates a delay in transport. A larger velocity profile in the momentum barrier layer is predicted by flow in restriction, which also refers to the case of a diminishing porous material.

Fig. 4 (a)-(b) and Fig. 7(a)-(b) illustrates an impact of slip parameter λ on velocity profile while considering distinct cases of K values. So, for 2nd order liquid, there are two regions of a with dual similarity solutions. There are two crucial values for λ. likewise, if λ exceeds or falls below specified essential limits. Thus the dual results are achieved. From Fig. 4(a)-(b) and Fig. 7(a)-(b) we can see that the magnitude of λ is increased, the fluid velocity drops. In the second approach of 2nd order liquid, fluid velocity declines as the slip quantity develops, while the first solution branch exhibits the opposite impact. It is evident that a higher value of λ suggests a lesser velocity, then stretching velocity partially transferred to the fluid.

However, in Fig. 8(a)-(c) and Fig. 9(a)-(b), momentum and non-dimensional stream function are exhibited for distinct values of K, Da^{-1} with λ. Regarding Walter's B scenario, the surface drag grows with the strength of K, Da^{-1} as well as λ second branch. Similar factors that affected viscoelastic in the second grade, it identifies inverse Darcy as well as slip factors. Whereas reverse effect is observed for 1st solution.

Since other factors are fixed, Fig. 10 describes the extent of the viscoelastic variable K on the skin friction coefficient profiles. The flow response to the normal stress coefficient is indicated by the viscoelastic component K. The flow skin friction coefficient profiles are seen to

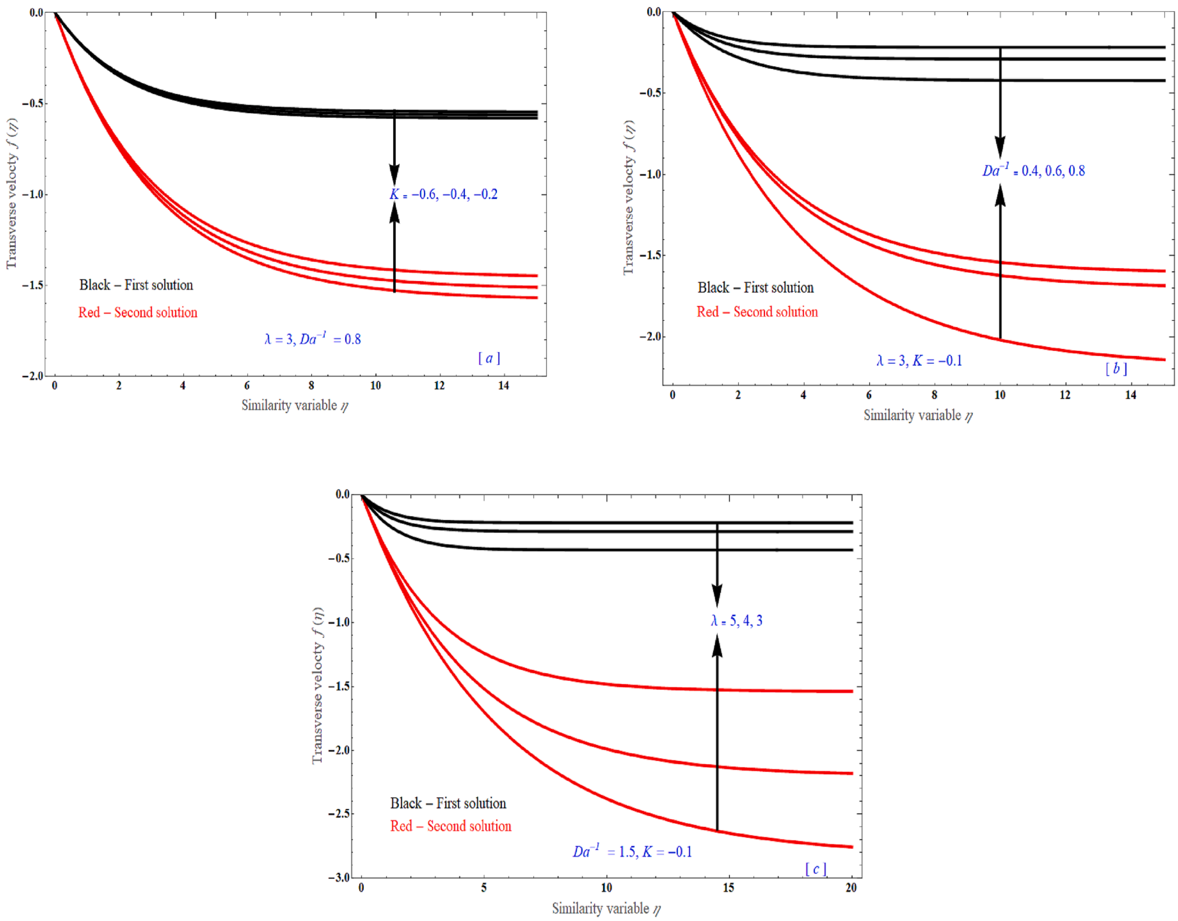

Fig. 9. An impact of (a) viscoelastic parameter K (b) inverse Darcy parameter Da^{-1} and (c) Navier slip λ on transverse velocity.

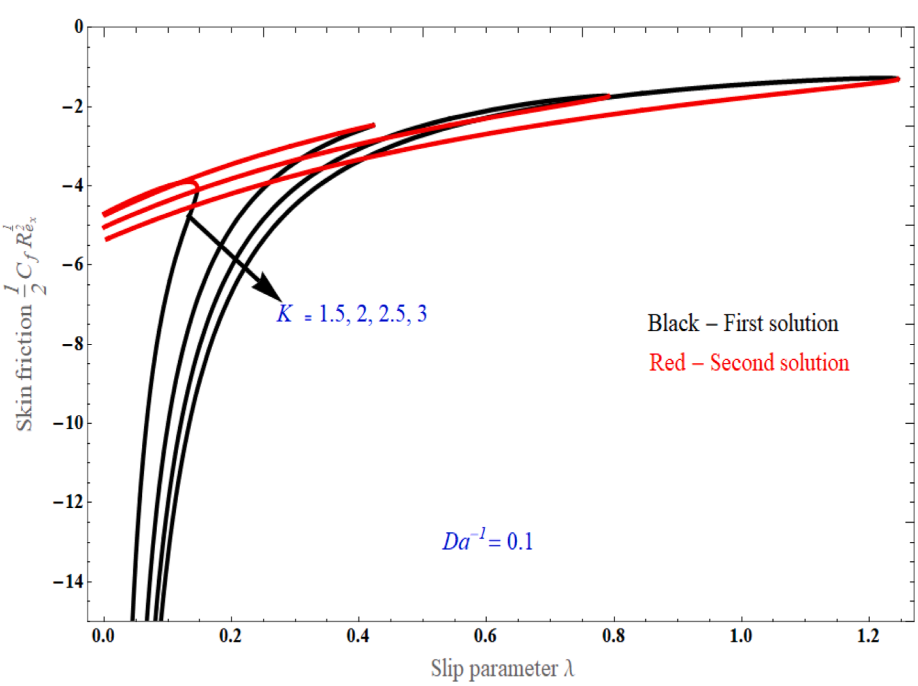

Fig. 10. Skin friction against slip parameter for various values of viscoelastic parameter K.

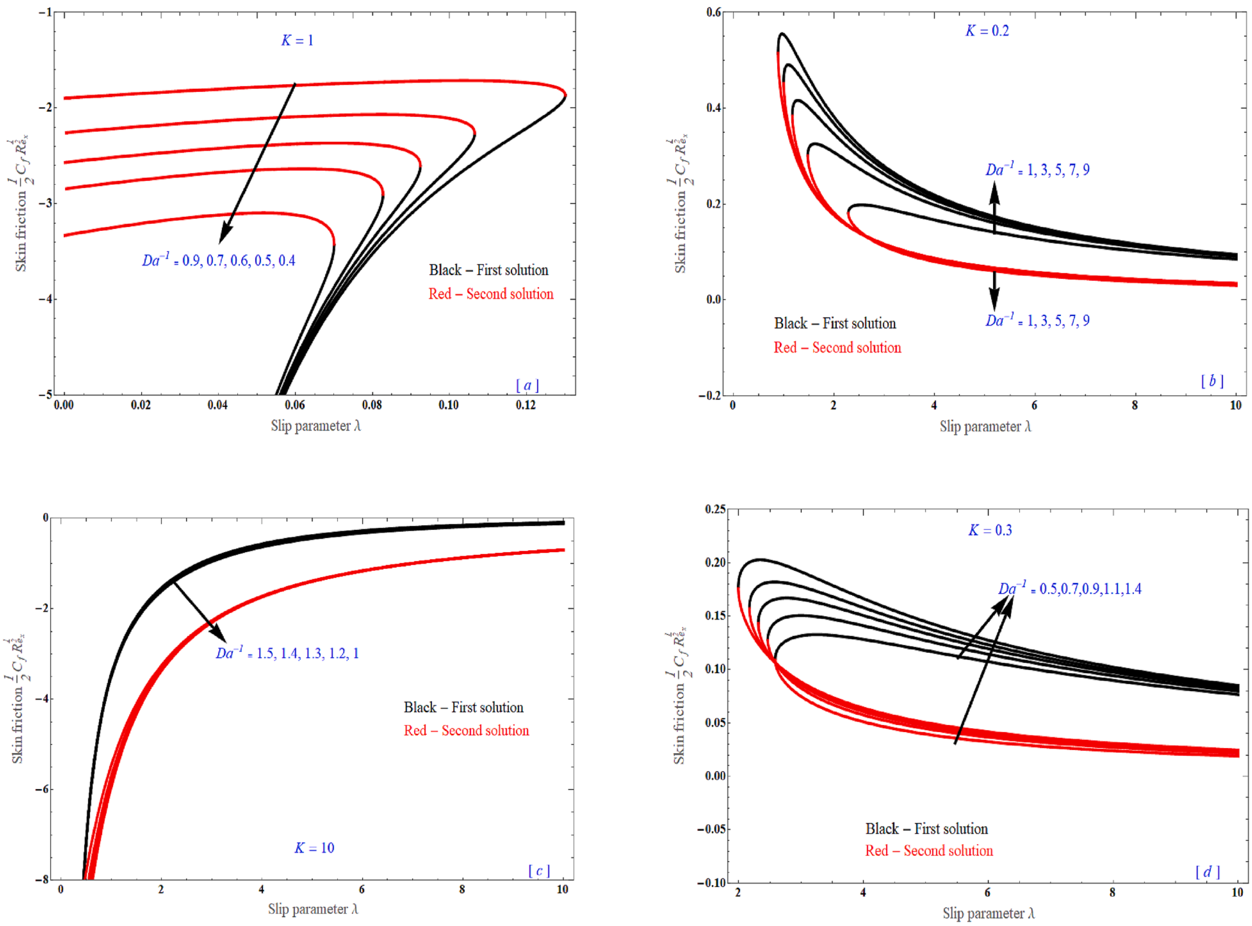

Fig. 11. An impact of inverse Darcy parameter on skin friction profile with (a) $K = 1$(b) $K = 0.2$(c)$K = 10$ and (d)$K = 0.3$.

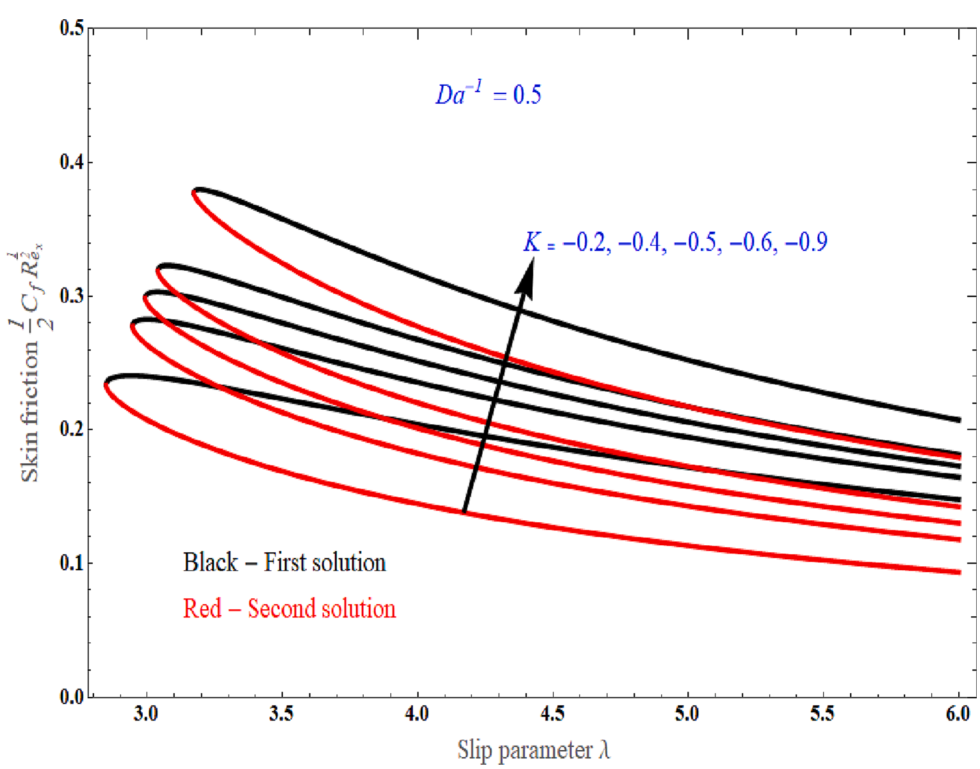

Fig. 12. Skin friction against slip parameter for various values of viscoelastic parameter K.

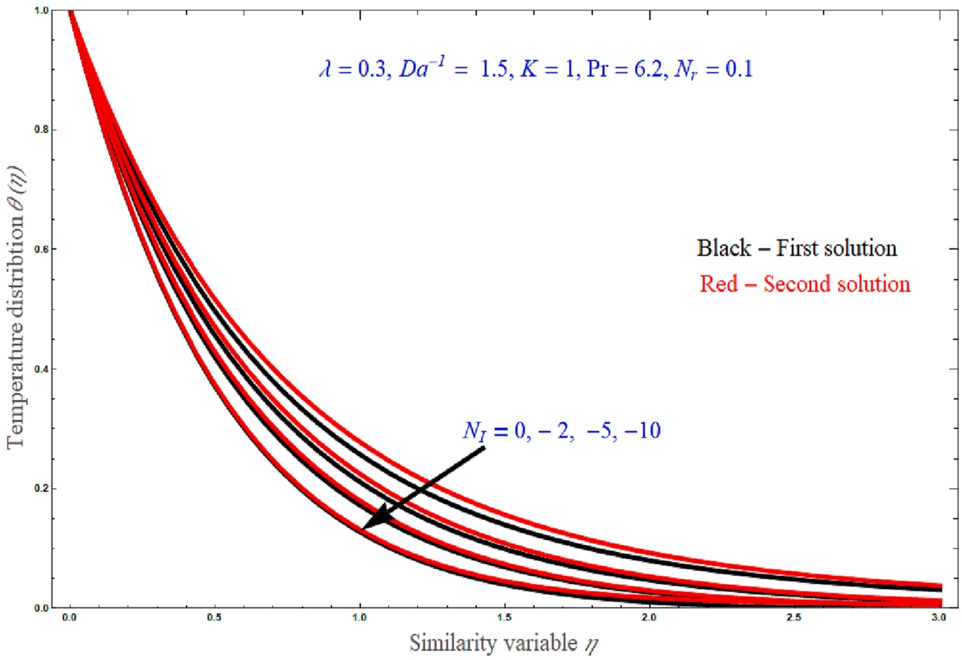

Fig. 13. An impact of heat source/sink parameter on temperature profile.

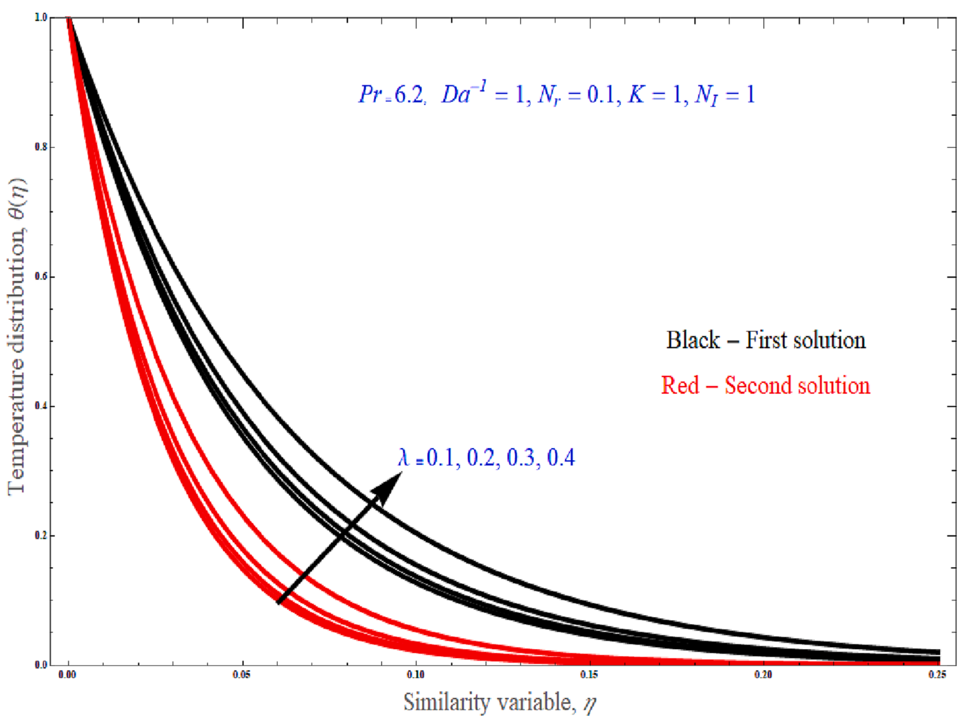

Fig. 14. An impact of slip parameter on temperature profile.

decline at a specific location on the flow domain, the viscoelastic component rises exponentially. Additionally, illustrations of skin friction displaying double, single, as well as no solutions are provided.

Figures11 (a)-(d) examines an effect of the inverse Darcy number patterns upon skin friction profile for various instances of. It is noticed that as the invers Darcy quantity falls, there is a reinforcement for surface velocity fluctuations, and so as a consequence, the skin friction coefficient is also drops.

Figure 12. illustrates the impact of the viscoelastic parameter (Walter's liquid B) K upon skin friction, for several viscoelastic parameter values, the skin friction coefficients have been plotted against the slip parameter. With an expansion in the viscoelastic parameter (Walter's liquid B), it's indeed evident that the skin friction boundary layer decrease.

Fig. 13 highlights the relationship between the heat source/sink component as well as the non - dimensional temperature profile. It is evident that raising the quantities of $N_I > 0$ emits energy, which raises the temperature, whilst increasing the ranges of $N_I < 0$ consumes energy, which diminishes the thermal field. Additionally, it's observed that the temperature distribution is greater whenever radiation phenomenon

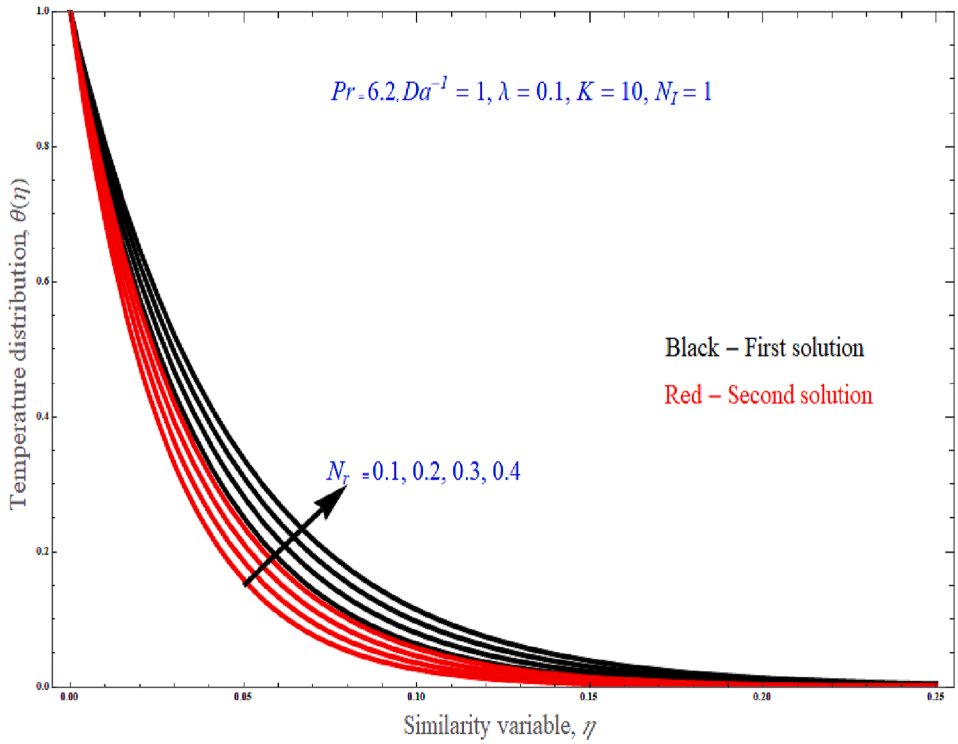

Fig. 15. An impact of radiation parameter on temperature profile.

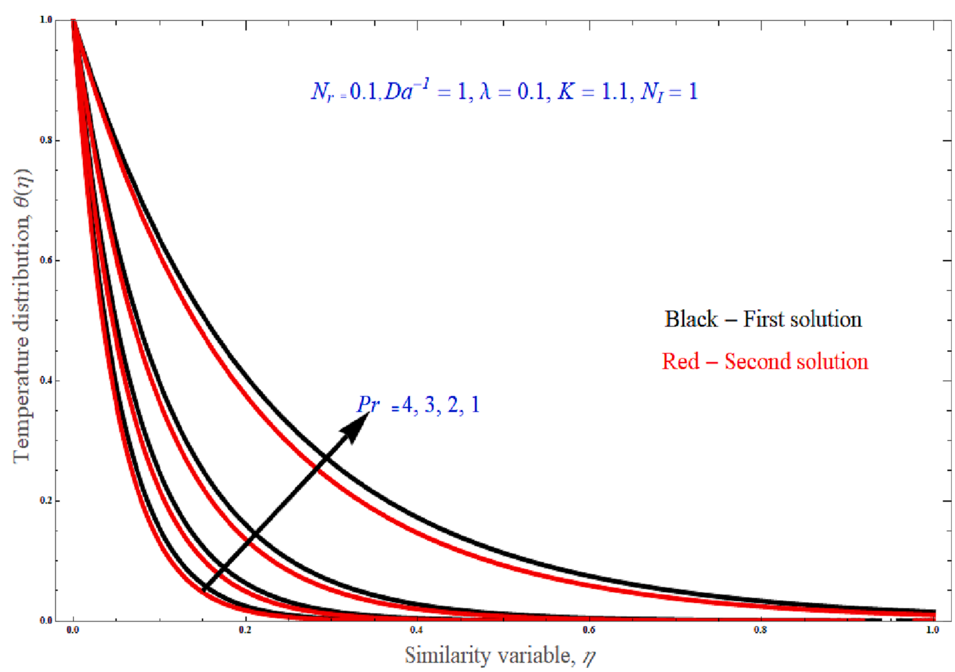

Fig. 16. An impact prandtl number on temperature profile.

is present, reason behind this is that adding radiation heat to the liquid more, intensifying the fluid temperature as well as width of barrier - layer. Fig. 14 displays how the slip parameter determines the temperature distribution for heated shrinking surface. The temperature profile improves in a specific initial region of η with higher slip parameter.

An effect of radiation upon temperature distribution depicted in Fig. 15. According to the graph, the finding implies that R value goes up, leading to a rise in wall temperature as well. This is highlighted by the fact that a higher radiation parameter promotes greater heat transfer through the liquid. Fig. 16 demonstrates that the fluid temperature is dropping in opposition to the Prandtl number *Pr*. This suggests that, contrary via magnitude of *Pr*, temperature barrier layer viscosity diminishes. This is mostly owing to relationship between a high Prandtl number and poor thermal diffusivity, which results in a smaller thermal barrier. In actuality, a rise in the fluid viscosity is signified by an acceleration in the *Pr*, and this, in turn, given rise to deterioration of thermal field. As a result, Prandtl number can be implemented to enhance efficiency of lowering of flows. Consequence of solid volume

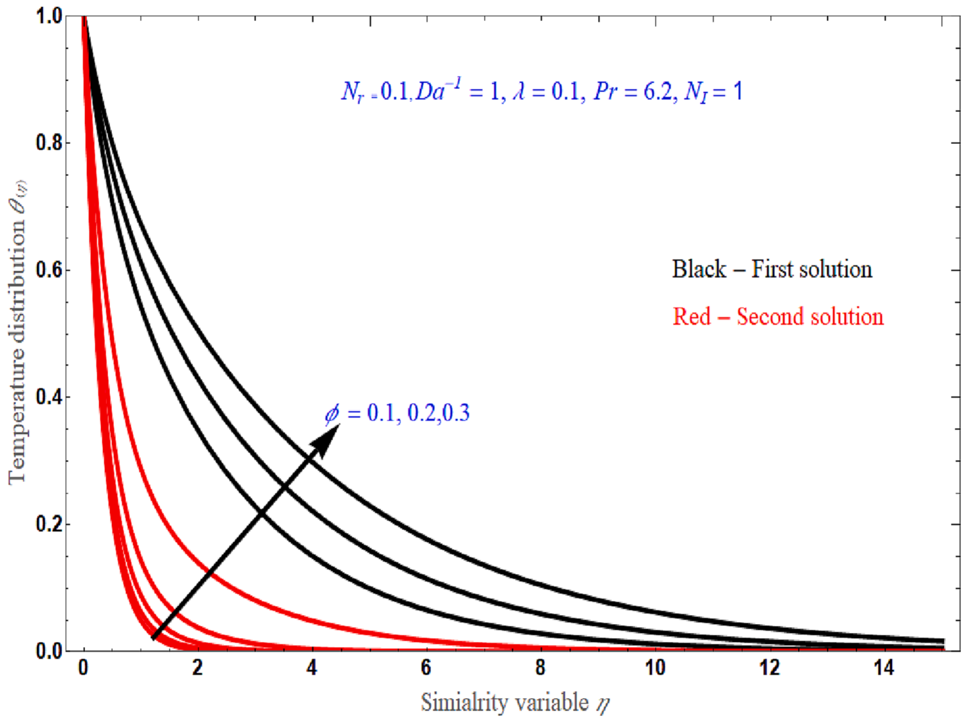

Fig. 17. An impact of solid volume fraction on temperature profile.

fraction on the temperature field is displayed in Fig. 17. Graph demonstrates that temperature profile climbs as that of the nanoparticle volume fraction improves. Since this is the case, both nanofluids possess lesser heat capacity as well as greater thermal conductivity when comparison to base liquid water, which promotes a progressive in thermal pattern.

Conclusions

The current study concerns the 2D motion of viscoelastic ternary nanofluid consisting of Silver (Ag)-SWCNTs-Graphene over a permeable shrinking surface has been investigated when exposed to radiation, slip parameter, and heat source/sink consequences. Through use of a similarity transformation, the dominating equations are modelled by a set of nonlinear ODEs, and are solved analytically via confluent hypergeometric function. The reported outcomes are in excellent agreement with the previously existing information. Following list provides some key findings from the current study:

- Dual solutions for the motion of the viscoelastic fluids arise for a specific range of the related parameter values.
- For the case of second grade fluid, whenever the slip parameter crosses a specific critical value, dual solutions happen for $K < 1$. However, for $K > 1$, there are two regions where dual solutions are found, and as K rises, dual responses are existent for all positive slip parameter values.
- With a decline in the width of the barrier layer, the magnitudes of K as well as λ grows in the first solution. Whereas, in 2nd solution region reverse effect is observed. In temperature field both K and λ values enhances with improving in thermal layer.
- Momentum profiles reduce as the inverse Darcy number rises in the both solutions.
- The internal heat source/sink may enhance or damps heat transfer.
- The temperature border layer's width is observed to be reduced by the Prandtl number.
- Thermal layer improved as enhances in magnitude of solid volume fraction.

The present investigation is limited by a several of preceding works:

i. $\lim_{T,\phi\to 0}$ {our results}→{results of Gautam[32] (2022)}.
ii. when there is no magnetic field, Q_0 as well as ϕ, {our results}→(results of Maranna et al [34](2022)}.

CRediT authorship contribution statement

T. Maranna: Conceptualization, Investigation, Methodology, Writing – review & editing. **U.S. Mahabaleshwar:** Supervision, Conceptualization, Methodology, Formal analysis, Writing – original draft, Writing – review & editing. **L.M. Pérez:** Methodology, Writing – review & editing. **O. Manca:** Supervision, Methodology, Writing – review & editing.

Declaration of Competing Interest

The authors declare that they have no known competing financial interests or personal relationships that could have appeared to influence the work reported in this paper.

Data availability

Data will be made available on request.

Acknowledgments

L.M.P. acknowledges partial financial support from ANID through Convocatoria Nacional Subvención a Instalación en la Academia Convocatoria Año 2021, Grant SA77210040. Also, Dr. U.S. Mahabaleshwar is thankful to University of Tarapaca for his hospitality during his stay at the University of Tarapaca, Chile.

References

[1] R. Ekiciler, Effects of novel hybrid nanofluid (Tio2-Cu/EG) and geometrical parameters of triangular rib mounted in a duct on heat transfer and flow characteristics, J Therm Anal Calorim. 143 (2) (2020) 1371–1387.
[2] L.S. Sundar, K.V.V. Chandra Mouli, Z. Said, A.C.M. Sousa, Heat transfer and second law analysis of ethylene glycol-based ternary hybrid nanofluid under laminar flow, J Therm Sci Eng Appl. 13 (5) (2021) 1–15.
[3] T. Elnaqeeb, I.L. Animasaun, A.S. Nehad, Ternary-hybrid nanofluids: significance of suction and dual-stretching on three-dimensional flow of water conveying nanoparticles with various shapes and densities, Zeitschrift Fur Naturforschung A 76 (03) (2021) 231–243.
[4] M. Sahu, J. Sarkar, L. Chandra, Steady-state and transient hydrothermal analyses of single-phase natural circulation loop using water based tri-hybrid nanofluids, AIChE J. 67 (6) (2021) e17179.
[5] Y. Xuan, W. Roetzel, Conceptions for heat transfer correlation of nanofluids, Int. J. Heat Mass Transf. 43 (19) (2000) 3701–3707.
[6] Y. Xuan, Q. Li, Heat transfer enhancement of nanofluids, Int. J. Heat Fluid Flow. 21 (1) (2004) 58–64.
[7] Z. Li, U. Khaled, A.A. Al-Rashed, M. Goodarzi, M. Sarafraz, R. Meer, Heat transfer evaluation of a micro heat exchanger cooling with spherical carbon-acetone nanofluid, Int. J. Heat Mass Transfer 149 (2020), 119124.
[8] A.D. Dhass, N. Beemkumar, S. Harikrishnan, H.M. Ali, A Review on Factors Influencing the Mismatch Losses in Solar Photovoltaic System, Int. J. Photoenergy. 2022 (2022) 1–27.
[9] T. Maranna, U.S. Mahabaleshwar, M.I. Kopp, An impact of Marangoni convection and radiation on flow of ternary nanofluid in a porous medium with mass transpiration. J. Appl. Comput. Mech.2023, 1–11. 10.22055/jacm.2022.41405.3748.
[10] K.N. Sneha, G.P. Vanitha, U.S. Mahabaleshwar, D. Laroze, Effect of couple stress and mass transpiration on ternary hybrid nanoliquid over a stretching/shrinking sheet with heat transfer, Micromachines 13 (2022) 1694.
[11] T. Gul, A. Saeed, Nonlinear mixed convection couple stress tri-hybrid nanofluids flow in a Darcy-Forchheimer porous medium over a nonlinear stretching surface, Waves Random Complex Media 1–18 (2022).
[12] S. Manjunatha, V. Puneeth, B.J. Gireesha, A.J. Chamka, theoretical study of convective heat transfers in ternary nanofluid flowing past a stretching sheet, J. Appl. Comput. Mech. 8 (2022) 1279–1286.
[13] F.A. Aamina, I. Khan, N.A. Sheikh, M. Gohar, I. Tlili, Effects of different shaped nanoparticles on the performance of engine-oil and kerosene-oil: A generalized brinkman-type fluid model with non-singular kernel, Sci. Rep. 8 (1) (2018) 15285.
[14] N.S. Khan, Magnetohydrodynamic nanoliquid thin film sprayed on a stretching cylinder with heat transfer, Appl. Sci. 7 (3) (2017) 271.
[15] N.A. Sheikh, D.L.C. Ching, I. Khan, A comprehensive review on theoretical aspects of nanofluids: Exact solutions and analysis, Symmetry. 12 (5) (2020) 725.
[16] B.C. Sakiadis, Boundary layer behavior on continuous solid surfaces: II. Boundary layer behavior on continuous fat surfaces. AICHE. 7(1961), 221–225.
[17] L.J. Crane, Flow past a stretching plate, J. Appl. Math. Phys. 21 (1970) 645–647.
[18] P.G. Siddheshwar, U.S. Mahabaleshwar, Effects of radiation and heat source on MHD flow of a viscoelastic liquid and heat transfer over a stretching sheet, Int. J. Nonlinear Mech. 40 (2005) 807–820.
[19] U.S. Mahabaleshwar, K.R. Nagaraju, P.N. Vinay Kumar, N.A. Kelson, An MHD Navier's slip flow over axisymmetric linear stretching sheet using differential transform method, Int. J. Appl. Comput. Math. 4 (1) (2017) 30.
[20] K. Suneetha, S.M. Ibrahim, P. Vijaya Kumar, K. Jyothsna, Linear thermal radiation effects on MHD viscoelastic fluid flow through porous moving plate with first order chemical reaction, variable temperature and concentration, J. Comput. Appl. Res Mech. Eng. 10 (2) (2021) 496–509.
[21] T. Hayat, Z. Abbas, M. Sajid, On the analytic solution of magnetohydrodynamic flow of a second grade fluid over a shrinking sheet, J. Appl. Mech. 74 (2007) 1165–1171.
[22] K.R. Rajagopal, T.Y. Na, A.S. Gupta, Flow of a viscoelastic fluid over a stretching sheet, Rheol. Acta. 23 (1984) 213–215.
[23] M. Emad, A. Eladahab, A. Mohamed El, Aziz, Blowing/suction effect on hydromagnetic heat transfer by mixed convection from an inclined continuously stretching surface with internal heat generation/absorption, Int. J. Therm. Sci. 43 (2004) 709–719.
[24] A. Raptis, Technical note: flow of a micropolar fluid past continuously moving plate by the presence of radiation, Int. J. Heat Mass Transf. 41 (1998) 2865–2866.
[25] A. Raptis, Radiation and viscoelastic flow, Int. Comm. Heat Mass Transf. 26 (6) (1999) 889–895.
[26] G. Sriharan, S. Harikrishnan, H.M. Ali, Enhanced heat transfer characteristics of the mini hexagonal tube heat sink using hybrid nanofluids, Nanotechnology 33 (2022), 475403.
[27] U.S. Mahabaleshwar, K.R. Nagaraju, P.N.V. Kumar, M.N. Azese, Effect of radiation on thermosolutal Marangoni convection in porous medium with chemical reaction and heat source/sink, Phys. Fluids. 32 (2020), 113602.
[28] D. Dey, O.D. Makinde, R. Borah, Analysis of Dual Solutions in MHD Fluid Flow with Heat and Mass Transfer Past an Exponentially Shrinking/Stretching Surface in a Porous Medium, Int. J. Appl. Comput. Math. 8 (66) (2022).
[29] D.H. Babu, N. Tarakaramu, P.V.S. Narayana, G. Sarojamma, O.D. Makinde, MHD flow and heat transfer of a Jeffrey fluid over porous stretching/shrinking sheet with a convective boundary condition, Int. J. Heat Technol. 39 (2021) 885–896.
[30] F.B. Tadesse, O.D. Makinde, L.G. Enyadene, Mixed convection of a radiating magnetic nanofluid past a heated permeable stretching/shrinking sheet in a porous medium, Math. Probl. Eng. (2021), https://doi.org/10.1155/2021/6696748.
[31] F.B. Tadesse, O.D. Makinde, L.G. Enyadene, Hydromagnetic stagnation point flow of a magnetic ferrofluid past a convectively heated permeable stretching/shrinking sheet in a Darcy-Forchheimer porous medium, Sadhana 46 (2021) 115.
[32] S.A. Jamuna, M.G. Murtaza, M. Ferdows, O.D. Makinde, K. Zaimi, Dual solutions analysis of melting phenomenon with mixed convection in a nanofluid flow and heat transfer past a permeable stretching/shrinking sheet, J. Nanofluids. 9 (2020) 313–320.
[33] K.S. Tshivhi, O.D. Makinde, Magneto-nanofluid coolants past heated shrinking/stretching surfaces: Dual solutions and stability analysis, Results Eng. 10 (2021), 100229.
[34] O.D. Makinde, V.B. Awati, N.M. Bujurke, Dirichlet series and closed form exact solutions of MHD casson fluid flow over a permeable stretching/shrinking sheet, Palestine Journal of Mathematics 10 (1) (2021) 109–119.
[35] S. Nadeem, T. Hayat, M.Y. Malik, S.A. Rajput, Thermal radiation effects on the flow by an exponential stretching surface: a series solution, Z. Naturforsch. 65A (2010) 495–503.
[36] R.C. Bataller, Viscoelastic fluid flow and heat transfer over a stretching sheet under the effects of a non-uniform heat source, viscous dissipation and thermal radiation, Int J Heat Mass Transfer. 50 (2007) 3152–3162.
[37] R. Cortell, Toward an understanding of the motion and mass transfer with chemically reactive species for two classes of viscoelastic fluid over a porous stretching sheet, Chem Eng Process. 46 (2007) 982–989.
[38] B. Mahantesh, B.J. Gireesh, R.S.R. Gorla, Heat and mass transfer effects on the mixed convective flow of chemically reacting nanofluid past a moving/stationary vertical plate, Alex. Eng. J. 55 (2016).
[39] A.K. Gautam, S. Rajput, K. Bhattacharyya, A.K. Verma, M.G. Arif, A.J. Chamkha, Existence of multiple solution for magnetohydrodynamics flows of second-grade and Walters's B fluids due continuously contracting flat sheet with partial slip, Partial. Differ. Appl. Math. 6 (2022), 100434.
[40] T. Anusha, U.S. Mahabaleshwar, M. Hatami, Navier slip effect on the thermal flow of Walters' liquid B flow due to porous stretching/shrinking with heat and mass transfer, Case Stud. Therm. Eng. 28 (2021), 101691.
[41] T. Maranna, K.N. Sneha, U.S. Mahabaleshwar, B. Souayeh, An impact of heat and mass transpiration on magnetohydrodynamic viscoelastic fluid past a permeable stretching/shrinking sheet, Heat Transf. (2022) 1–18.
[42] T. Fang, J. Zhang, Closed-form exact solutions of MHD viscous flow over a shrinking sheet, Comm Nonlinear Sci Num Simul. 14 (7) (2009) 2853–2857.
[43] N.C. Roy, I. Pop, Dual solutions of magnetohydrodynamic mixed convection flow of an Oldroyd's-B nanofluid over a shrinking sheet with heat source/sink, Alexandria Eng J. 61 (8) (2021) 5939–5948.
[44] A.B. Vishalakshi, T. Maranna, U.S. Mahabaleshwar, D. Laroze, An Effect of MHD on Non-Newtonian Fluid Flow over a Porous Stretching/Shrinking Sheet with Heat Transfer, Appl. Sci. 12 (2022) 4937.
[45] U.S. Mahabaleshwar, T. Maranna, F. Sofos, Analytical investigation of an incompressible viscous laminar Casson fluid flow past a stretching/shrinking sheet, Sci. Rep. 12 (2022) 18404.
[46] T. Maranna, K.N. Sneha, U.S. Mahabaleshwar, I.E. Sarris, T.E. Karakasidis, An effect of radiation and MHD Newtonian fluid flow over a stretching/shrinking sheet with CNTs and mass transpiration, Appl. Sci. 12 (2022) 5466.
[47] M. Darzi, M. Vatani, S.E. Ghasemi, Effect of thermal radiation on velocity and temperature fields of a thin liquid film over a stretching sheet in a porous medium, Eur. Phys. J. Plus. 130 (2015) 100.
[48] M. Sahu, J. Sarkar, Steady-state energentic and exergetic performance of single phase natural circulation loop with hybrid nanofluids, J. Heat Transfer. 141 (8) (2019), 082401.
[49] A.S. Nehad, I.L. Animasaun, A. Wakif, O.K. Koriko, R. Sivaraj, K.S. Adegbie, Z. Abdelmalek, H. Vaidya, A.F. Ijirimoye, K.V. Prasad, Significance of suction and dual stretching on the dynamics of various hybrid nanofluid: comparative analysis between type I and type II models, Phys. Scr. 95 (9) (2020), 095205.
[50] B. Takabi, S, Saleh, Augmentation of the heat transfer performance of a sinusoidal corrugated enclosure by employing hybrid nanofluid, Advanced. Mech. Eng. 16 (2014), 147059.
[51] K. Kalidasan, L.R. Velkennedy, P.R. Kanna, Laminar natural convection of copper-titania/water hybrid nanofluid in an open ended – C- shaped enclosure with an Isothermal block, J. Mol. Liq. 246 (2017) 251–258.
[52] S. Saleem, I.L. Animasuan, S.J. Yook, Q.M. Al-Mdallal, N.A. Shah, M. Faisal, Insight into the motion of water conveying three kinds of nanoparticles on a horizontal surface: significance of thermos-migration and Brownian motion of different nanoparticles. Surf and interface, 2022.
[53] C. Kleinstreuer, Y. Feng, Experimental and theoretical studies of nanofluid thermal conductivity enhancement: A review, Nanoscale Res Lett. 6 (2011) 229.
[54] H. Liu, I.L. Animasaun, N.A. Shah, O.K. Koriko, B. Mahanthesha, Further discussion on the significance of quartic auto catalysis on the dynamics of water conveying 47nm alumina and 29 nm cupric particles, Arab. J. sci. Eng. 45 (7) (2016) 5977–6004.
[55] T. Hayat, S. Qayyum, M. Imtiaz, A. Slaedi, comparative study of silver and copper water nanofluids with mixed convection and non-linear thermal radiation, Int. J. Heat mass transf. 102 (2016) 723–732.